Available online at www.sciencedirect.com
ScienceDirect
Trans. Nonferrous Met. Soc. China 31(2021) 3024−3038
Transactions of Nonferrous Metals Society of China
www.tnmsc.cn

Comparative investigation on copper atmospheric corrosion by electrochemical impedance and electrical resistance sensors

Shan WAN[1], Bo-kai LIAO[1], Ze-hua DONG[2], Xing-peng GUO[1, 2]

1. School of Chemistry and Chemical Engineering, Guangzhou University, Guangzhou 510006, China;
2. Hubei Key Laboratory of Material Chemistry and Service Failure, School of Chemistry and Chemical Engineering, Huazhong University of Science and Technology, Wuhan 430074, China

Received 9 January 2021; accepted 30 June 2021

Abstract: Electrochemical impedance (EIS) and thin electrical resistance (ER) sensors were invented for atmospheric corrosion measurement of copper (Cu) during cyclic wetting−drying/high−low temperature tests and field exposure tests. Three-month field exposure results showed that average corrosion rate of Cu measured by ER sensor was well in accordance with that by weight loss method. During cyclic wetting−drying test, EIS was proven to reflect sensitively time of wetting and drying on the surface of sensor. Although corrosion rate obtained from EIS had a similar tendency to that obtained from ER sensors, the former was more dependent on environmental humidity than the latter. When relative humidity was low than 60%, corrosion rate of Cu measured by EIS was much lower than that by weight loss method, mainly attributing to the fact that impedance sensor failed to detect corrosion current of interlaced Cu electrodes due to the breakdown of conductive passage composed of absorbed thin liquid film under low humidity condition. Promisingly, ER sensor was proven to be more suitable for atmospheric corrosion monitoring than electrochemical techniques because it could sensitively monitor thickness loss of Cu foil according to the Ohmic law, no matter how dry or wet the sensor surface is.

Key words: atmospheric corrosion; copper; electrical resistance probe; electrochemical impedance; in-situ corrosion monitoring

1 Introduction

Copper is the most widely used electronic interconnecting metal due to its excellent electrical conductivity, thermal conductivity and corrosion resistance [1−4]. When electronic equipment serves in harsh environments, such as marine atmospheric environment [5−8], some gas pollutants or salt particles may absorb or deposit on the surface of printed circuit board (PCB) owing to the poor air filtration, leading to corrosion of pins, solder plate and even leads of integrated chip on the PCB [9−12]. With the developing integration and miniaturization of electrical components, ng-level corrosion loss could lead to failure of whole electrical circuits [13−15]. Generally, atmospheric corrosion behavior of PCB-Cu begins with the formation of microdroplets due to the deliquescence of salt particle [16,17]. In order to avoid the unexpected failure of microelectronics, it is vital to monitor the volatilization and condensation process of saline droplets as well as the corrosion of underlying PCB-Cu.

In the past few decades, galvanic-type corrosion sensors have been widely applied in the field of the atmospheric corrosion measurement (ACM) [18−22], which are composed of two heterogeneous metal electrodes and designed on the basis of galvanic amperometry. MANSFELD et al [23−25] firstly adopted the galvanic-cell Cu−Zn sensors to monitor atmospheric corrosivity,

Corresponding author: Ze-hua DONG, Tel: +86-27-87543432, E-mail: zhdong@hust.edu.cn
DOI: 10.1016/S1003-6326(21)65712-6

finding that it was difficult to detect flow current under the condition of discontinuous or extremely thin electrolyte layer. MIZUNO et al [26] studied the atmospheric corrosion of steel by Fe−Ag type sensors, aiming at monitoring atmospheric corrosivity through galvanic current. However, the galvanic current is generally measured at polarized rather than natural status, it only represents the atmospheric corrosivity, or time of wetting (TOW) rather than the realistic corrosion rate of metal electrodes. On the other hand, electrochemical impedance spectra (EIS), as a lowly disturbing corrosion measurement method, has been widely used in atmospheric corrosion measurement [27−29], where the impedance in high frequency (10 kHz) and low frequency regions (0.01 Hz) respectively represents the resistance of adsorbed thin electrolyte layer (TEL) and charge transfer. NISHIKATA et al [30] employed EIS to study atmospheric corrosion behaviors of metals by using two nominally identical mild steel electrodes in the wetting−drying cycling test, in which the two electrodes were covered by simulating TEL with different thicknesses. Nevertheless, the simulating TEL is much different from naturally formed TEL in the real atmosphere because the latter is usually discontinuous with a varying thickness. To simulate the atmospheric corrosion scenarios more realistically, LI et al [31] developed a two-electrode sensor to study atmospheric corrosion of weathering steel induced from deliquescence of NaCl particles, and found that EIS at different relative humidities (RH) often corresponded to different equivalent circuits. In our previous work [32], we studied the dewing process and atmospheric corrosion of Cu under cyclic wetting−drying test using a two-electrode system with comb-like arrangement. It is found that when the RH is low (for example 60%), the corrosion rate (<1 nm/a) calculated by the low-frequency impedance was much lower than the realistic rate (0.1−0.5 μm/a) of Cu owing to the lack of conductive passage (without continuous TEL) across two Cu electrodes. The above results suggest that the electrochemical techniques are not suitable for ACM.

Fortunately, the electrical resistance (ER) technique [33−35] could avoid the necessity of existing continuous TEL on metal samples, which calculates the corrosion rate of metal based on the Ohmic law other than the electrochemistry beneath TEL. If a metal stripe or wire is corroded, the thickness loss and corrosion rate could be deduced by measuring the tiny resistance change of metal specimen. CAI and LYON [36] applied ER probe to investigate the atmospheric corrosion kinetics of iron, and found that it is a rate-controlling process involving some regeneration of chloride ions. PROSEK et al [37] studied the corrosion of copper, bronze, and iron samples exposed to indoor atmosphere (80% RH) by automated electrical resistance sensors, and found that short-chain volatile carboxylic acids in air could significantly accelerate corrosion when their concentration is over 300×10^{-9} with 80% RH.

In this work, electrochemical impedance and ER techniques were combined to research the atmospheric corrosion of Cu in field exposure and wetting−drying/high−low temperature cycling tests. The corrosion rate of Cu obtained by weight loss method in the same atmosphere was used as a reference. The sensitivity, accuracy, as well as correlation and difference of two ACM methods were comparatively studied.

2 Experimental

2.1 Materials and reagents

Cu (>99.9 wt.%) coupons with size of 50 mm (width) × 100 mm (length) × 3 mm (thickness) were used for weigh loss test and the following surface analysis during ACM. Prior to the experiments, Cu coupons were ground with $800^{\#}$, $1000^{\#}$ and $1500^{\#}$ silicon carbide emery papers sequentially, then rinsed with anhydrous alcohol and acetone for 5 min in the ultrasonic cleaner, subsequently dried with cold air. Finally, all Cu coupons were stored in desiccator for no more than 24 h before use.

NaCl, acetone and anhydrous alcohol with analytical purity were provided by Sinopharm Chemical Reagent Co., Ltd. Deionized water was self-produced by the laboratory.

2.2 Atmospheric corrosion monitoring sensors

2.2.1 Electrical resistance sensor

ER sensor is made of thin Cu stripes attached on a PCB, and a CST480 datalogger (Corrtest Instruments, Wuhan, China) was employed to gauge the corrosion amount of Cu, as shown in Fig. 1. The ER datalogger applied a constant current

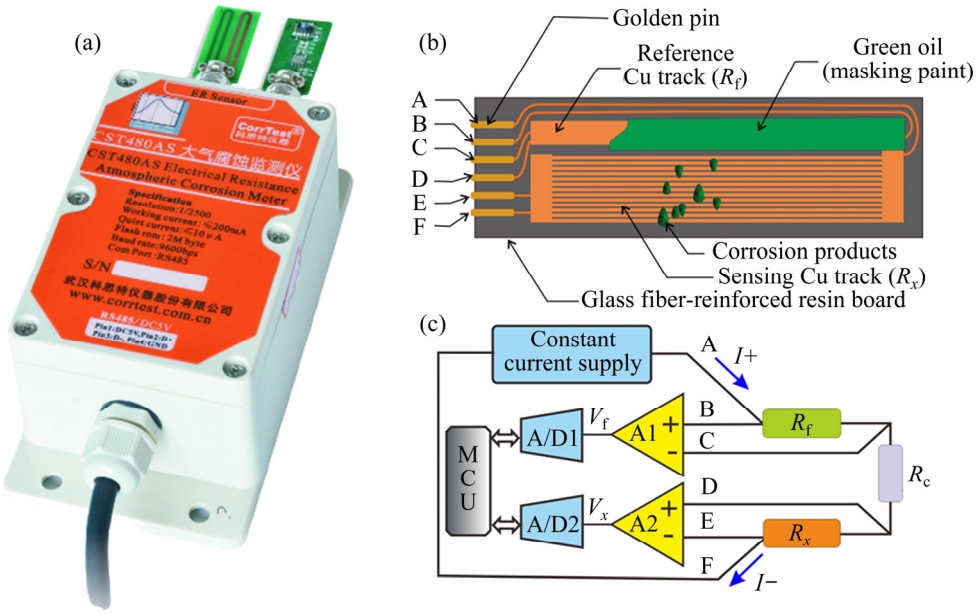

Fig. 1 Photograph (a), Cu sensor (b), and schematic electronic circuits (c) of electrical resistance datalogger

across the Cu stripes and measured the voltage drop between two terminals of the Cu stripes. The corrosion rate could be deduced from the derivative of thickness loss versus time, which was used for evaluating the atmospheric corrosion of Cu according to the ISO 9223—2012 standard. The ER sensor was prepared as follows: firstly, 35 μm-thick Cu stripes were plated on a glass fiber-reinforced epoxy resin sheet by etching method, to form a particular pattern consisting of 50 Cu tracks in parallel, among which 25 Cu tracks were exposed to air acting as sensing element, while the remaining 25 tracks were masked by green paint as reference element (Fig. 1(b)). Each Cu track is 5 cm in length and 100 μm in width, and the distance between each of Cu track is 100 μm.

ER datalogger is composed of a precise constant current source, two 24bit A/D converters and a thermocouple, as shown in Fig. 1(c), where Pin A and Pin F refer to current input and output terminals, Pin B and Pin C are used to sense the voltage drop across sensing track, and Pin D and Pin E are used to sense the voltage drop across the reference track. The current is firstly generated by the constant-current source to flow through R_x and R_f, and then the partial voltage V_x and V_f across R_x and R_f are measured by the two instrumental amplifiers and 24bit Σ-Δ A/D converter, respectively. The R_x/R_f ratio of λ is recorded chronologically. Considering that R_x is increased with time due to the corrosion of exposed tracks, the λ would increase with time. Thus, the corrosion thickness loss and corrosion rate of Cu could be deduced from the derivate dλ/dt.

Considering the plate-type sensing elements in ER sensor, the thickness d_x would decrease with undergoing corrosion, when a constant current I flows through Pin A to Pin F, accordingly the voltage drop (V_x) of sensing track is equal to IR_x, and V_f=IR_f. The voltage ratio (λ) could be calculated by

$$\lambda=\frac{V_x}{V_f}=\frac{IR_x}{IR_f}=\frac{\rho L_x}{\rho L_f}\frac{w_f d_f}{w_x d_x} \tag{1}$$

where L_x, w_x and d_x represent the length, width and thickness of exposed Cu tracks (sensing element), respectively, and L_f, w_f and d_f are the length, width and thickness of green oil masked Cu tracks (reference element), and ρ is the Cu resistivity. Allowing for that the width and length of the sensing and reference tracks are unchanged during the ACM period, at a certain time t, Eq. (1) could be simplified as

$$d_x(t)=\frac{C}{\lambda(t)} \tag{2}$$

$$C=d_f\frac{L_x}{L_f}\frac{w_f}{w_x} \tag{3}$$

Obviously, for a specific ER sensor, C is a

constant. Therefore, the residual thickness $d_x(t)$ at time t of the sensing track is inversely proportional to the ratio of voltage drop $\lambda(t)$ at the same time. The corresponding corrosion rate of exposed Cu track at time t could be deduced by differentiating thickness against time, as

$$r_{\text{corr}}(t) = -\frac{\delta d_x(t)}{\delta t} \quad (4)$$

2.2.2 Electrochemical impedance sensor

As shown in Fig. 2, the two-electrode configuration with comb-like (interlaced) Cu stripes plated on glass fiber enhanced resin laminate (Fig. 2(b)), which has been illustrated in our previous work [32]. A portable datalogger (impedance analyzer) was used to gauge the impedance of Cu electrodes on the comb-like sensor at two fixed frequencies, to obtain polarization resistance of Cu at 0.01 Hz and TEL resistance at 10 kHz, respectively. The corrosion current density and corrosion rate could be deduced according to the Stern−Geary equation [25]. The impedance datalogger can automatically carry out measurement according to preset time interval under the control of real-time clock (Fig. 2(c)). In this work, the measurement interval was set to be 1 h. The impedance datalogger can be easily used in field thanks to its mini size and low power consumption.

2.3 Procedure

2.3.1 Field exposure test

After pretreatments, all Cu coupons and ER sensor are installed in the atmospheric corrosion field station in Wuhan, China, at an inclination of 45° with respect to horizontal direction. The longitude and latitude of the exposure site are 114.41° and 30.51°, respectively. According to the meteorological data, the average temperature, relative humidity, Cl^- deposition amount, and SO_2 content are 23.1 °C, 61.5%, 1719 mg/cm^3 and 0.3342 mg/cm^3. To avoid the galvanic corrosion between different materials, the testing racks and bolts used for installation of Cu coupons were made of polytetrafluoroethylene. The ER datalogger was set to read data once 1 h. Five Cu coupons were retrieved once a month, and then corrosion products on their surfaces were cleaned by 10 wt.% amino sulfonic acid aqueous solution. The average corrosion rate of five Cu specimens was acquired by weight loss method.

2.3.2 Wetting−drying/high−low temperature cycling test

All wetting−drying/high−low temperature cycling tests were carried out in a programmable weathering chamber (YS−80−880S, Yi Shen, China), which could adjust temperature and relative humidity according to the preset procedure. The ER

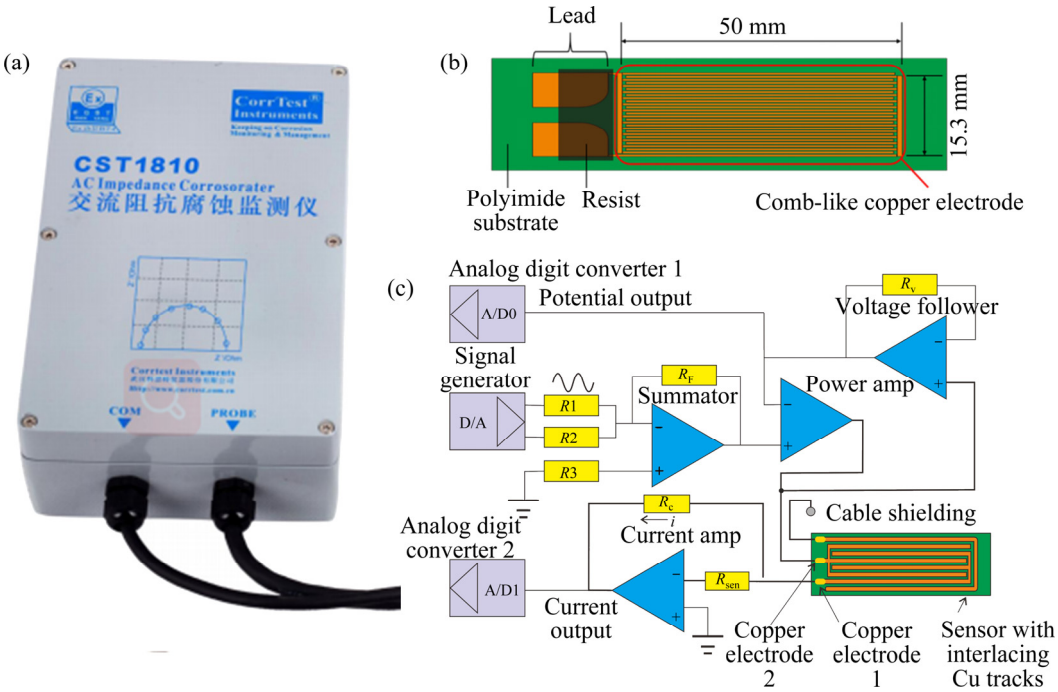

Fig. 2 Photograph (a), Cu comb-like electrode (b), and schematic electronic circuit (c) of electrochemical impedance datalogger

and impedance sensors were pre-deposited with 10 μg/cm^2 NaCl and then put in the weathering chamber.

The procedure of wetting−drying cycle is as follows: the air in the chamber was maintained at 35 °C with 90% RH (wetting period) for 2 h, and then it was quickly switched to 35 °C with 60% RH (drying period) for 4, 10, 16 and 22 h respectively, as shown in Fig. 3(a). The wetting−drying cycle repeats many times until total time reaches 168 h. Among the four kinds of wetting−drying cycling tests, the wetting period keeps unchanged, while the dry period increases in sequence.

The procedure of high−low temperature cycle is as follows: the air in the chamber was maintained at 45 °C with 60% RH (high temperature period) for 2 h, and then it was quickly switched to 25 °C with 60% RH (low temperature period) for 4, 10, 16 and 22 h, respectively, as shown in Fig. 3(b). The high−low temperature cycle was repeated until total time reached 168 h. Among the four kinds of high−low temperature cycling tests, the high temperature period keeps unchanged, while low temperature period increases in sequence.

2.4 Surface characterizations

The crystalline corrosion products were characterized by X-ray diffraction (XRD, PANalytical B.V., Holland) with a Cu K_α target under 50 kV, 250 mA and 2θ=10°−85° at a scanning speed of 2 (°)/min. The morphology of corrosion products was observed by field emission scanning electron microscopy (FESEM) equipped with 15 kV ion beam.

3 Results and discussion

3.1 Atmospheric corrosion at field exposure station

Cu coupons and ER sensors were installed simultaneously in the atmospheric exposure field on the 14th, August 2019. Figure 4 shows the time dependence of the resistance ratio (λ) and corrosion rate (CR) based on the ER sensors. It is seen that the instantaneous corrosion rate measured by ER sensor fluctuates a lot with time, which is mainly attributed to the alternate wetting and drying surface due to the rainfall and temperature variation between day and night. During the whole exposure period, the average corrosion rate of Cu measured by ER is ~0.6 μm/a. To verify the reliability of ER sensor, the atmospheric corrosion rate of Cu was simultaneously checked by weight loss method, and the corresponding corrosion rate results are listed in Table 1. It indicates that the measured corrosion rate obtained by the ER sensor is nearly consistent with that by weight loss method, suggesting that the ER sensor is rather reliable for outdoor ACM.

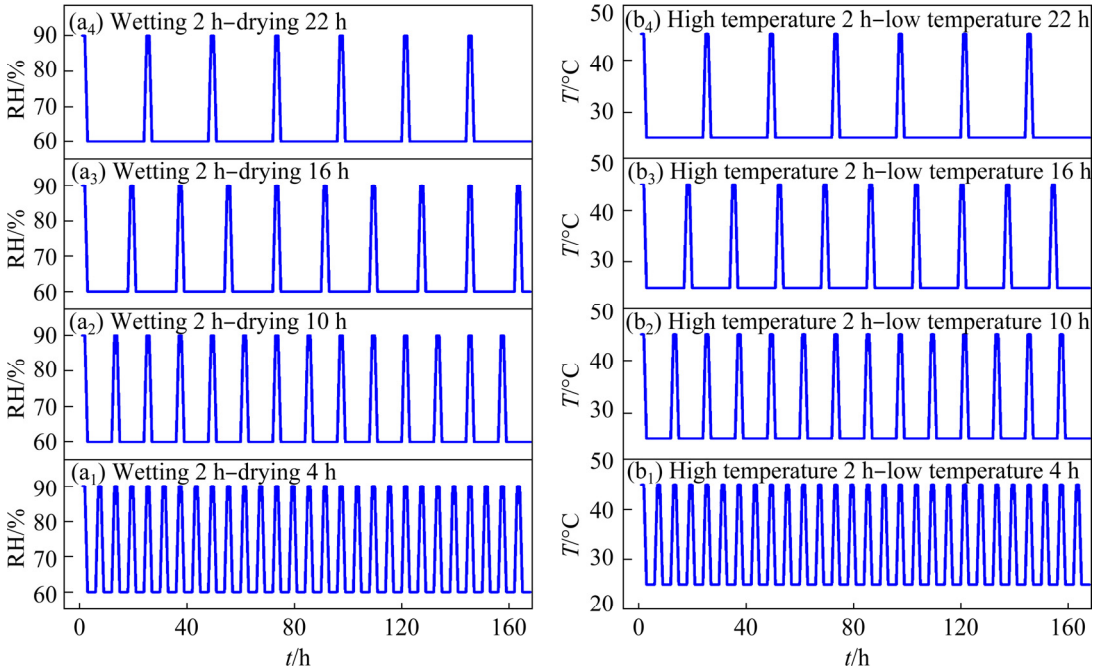

Fig. 3 Procedure diagrams of four kinds of wetting−drying cycling tests (a_1−a_4) and high−low temperature cycling tests (b_1−b_4)

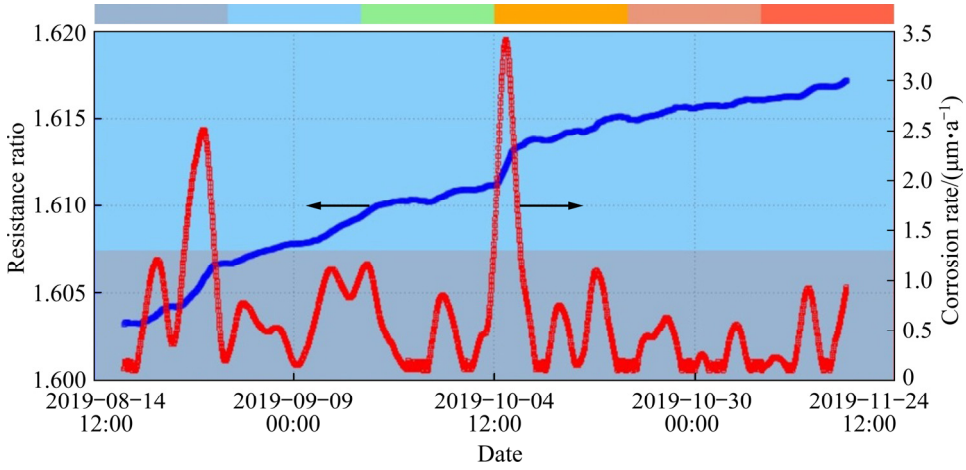

Fig. 4 Corrosion rate and resistance ratio measured by ER sensor in field atmospheric exposure station of Wuhan, China

Table 1 Comparison of copper corrosion rate results by weight loss and ER methods

Monitoring technique	Average corrosion rate/(μm·a^{-1})		
	30 d	60 d	100 d
Weight loss method	0.49±0.02	0.54±0.01	0.56±0.02
ER method	0.63±0.03	0.61±0.02	0.60±0.01

Figure 5 shows the corrosion rate measured by ER sensor during 60 d corrosion test in the weathering chamber. After the ER sensor with pre-deposited NaCl particles was exposed to 90% RH and 35 °C air, salt particles deliquesced quickly and formed microdroplets. Therefore, the initial corrosion rate is relatively higher and then it begins to decrease owing to the formation of corrosion products. When temperature increases from 35 to 45 °C, water vapor would quickly condense (dewing) on the surface of sensor due to the temperature difference between the sensor and the surrounding airflow inside the chamber. Owing to the thermal inertia of the sensor, the temperature of the sensor increases at a slower rate than that of airflow, which contributes to the formation of thickening TEL and accelerates the corrosion of underlying Cu. On the other hand, when the temperature decreases from 45 to 25 °C, the sensor surface would become dry during dehumidifying process (to sustain a constant RH), leading to a reduced corrosion rate.

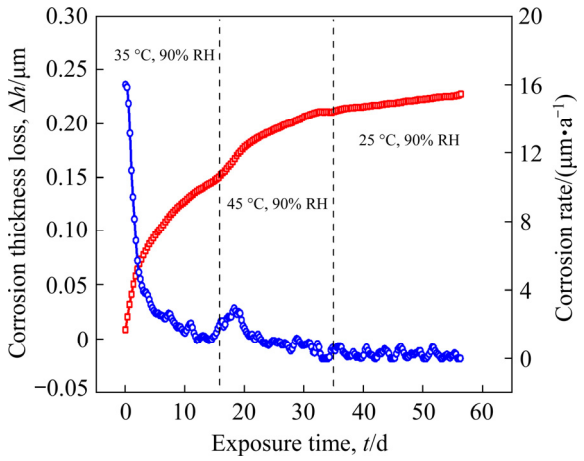

Fig. 5 Corrosion rate measured by ER sensor in accelerated corrosion test

3.2 Corrosivity of wetting−drying cyclic atmosphere

The accelerated atmospheric corrosion of Cu was conducted through wetting−drying cycling test, aiming at checking the consistency of EIS and ER techniques. Figure 3 shows the schematics of four accelerated wetting−drying/high−low temperature cycling tests, in which the corrosion of Cu was measured by impedance sensor (Fig. 6(a)) and ER sensor (Fig. 6(b)) simultaneously in the weathering chamber (Fig. 6(c)).

Impedance sensor could be used to measure the TEL resistance (R_s) and polarization resistance (R_p) between the interlaced Cu electrodes, while ER sensor is more suitable to the thickness loss measurement. The TEL resistance is mainly proportional to the wetness on Cu electrode surface, and R_p is to the reciprocal of corrosion rate according to the Stern−Geary equation. Figure 7 shows the time dependence of R_s of NaCl-contaminated Cu, firstly exposed in 90% RH and 35 °C air for 2 h, and then exposed in 60% RH and 35 °C air for 4 h (a), 10 h (b), 16 h (c) and 22 h (d), respectively. It could be obviously seen that the

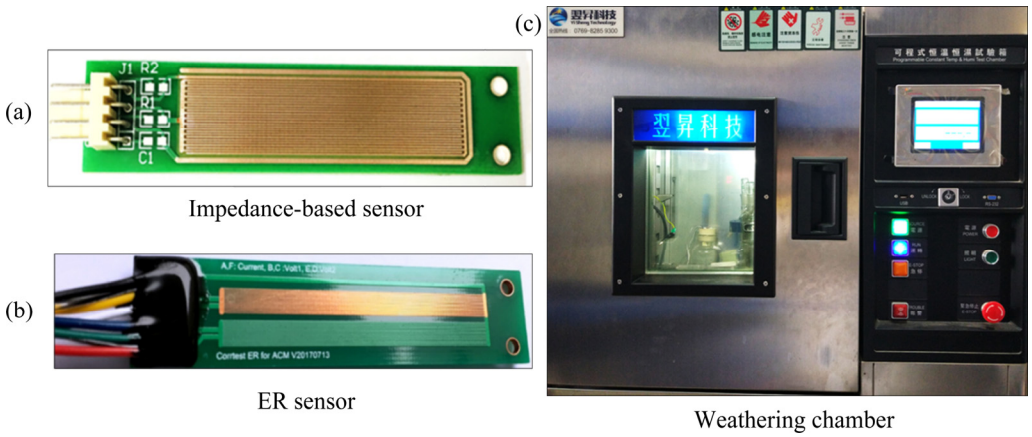

Fig. 6 Photographs of impedance sensor (a), ER sensor (b), and weathering chamber (c)

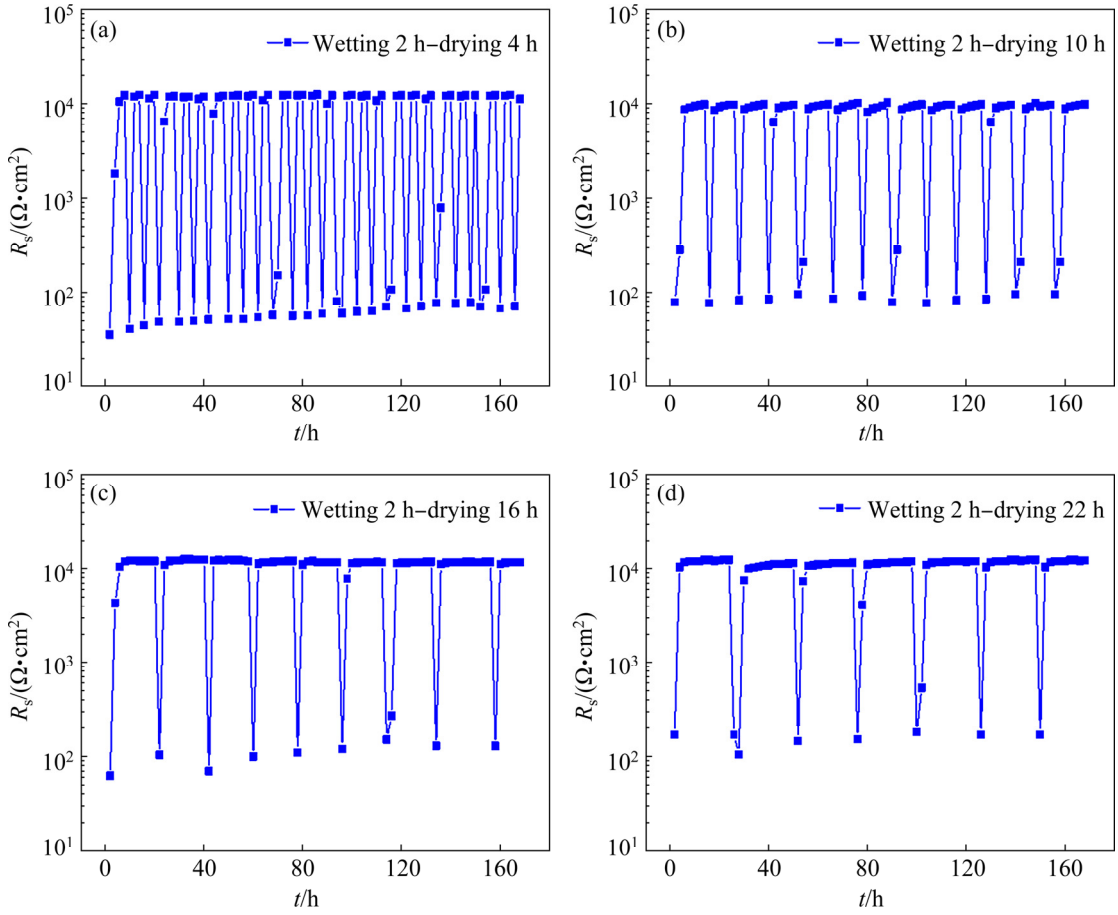

Fig. 7 Variations of liquid film resistance of NaCl-contaminated copper with time, firstly exposed in 90% RH and 35 °C air for 2 h, and then in 60% RH and 35 °C for 4 h (a), 10 h (b), 16 h (c) and 22 h (d) (The wetting−drying cycle repeats until total time reaches 168 h)

value of R_s during the wetting period is rather low, while it sharply increases during the drying period. Furthermore, the variations of R_s in the wetting and drying periods are exactly consistent to the timing of wetting−drying cycles (Fig. 3(a)), which suggests that impedance sensor could sensitively indicate the time of wetting (TOW) on the sensor surface. The TOW could be an indicator for the atmospheric corrosion prognostics and environmental corrosivity. Generally, the longer the TOW is, the severer the atmospheric corrosivity is [38]. However, the above criterion for estimating environmental corrosivity is

not always accurate, which could be evidenced by the following corrosion tests in Fig. 8.

Figure 8 summarizes the time dependance of corrosion rate of NaCl-contaminated Cu based on the impedance (a_1−a_4) and ER (b_1−b_4) sensors when exposed in 90% RH and 35 °C air for 2 h and then in 60% RH and 35 °C air for 4, 10, 16 and 22 h. The wetting−drying cycle is repeated until 168 h total time reaches. The R_p of Cu electrode was measured at low frequency (0.01 Hz), and then the corrosion rate (CR) was calculated by the Stern−Geary equation (CR=B/R_p, where B is the Stern−Geary coefficient, here it is assumed to be 50 mV). Meanwhile, the thickness loss of Cu stripe was estimated by ER sensor, and the corrosion rate of Cu is calculated by the time derivative of thickness loss. Comparing with the corrosion rate curves by EIS and ER sensors, it can be found that their trend against time is consistent, but the values of corrosion rate measured by the EIS sensor are much lower than those by the ER sensor in the same atmosphere, one of the reasons is that the ER mainly reflects the average corrosion rate but the EIS reflects the instant rate.

To compare the thickness loss differences from the EIS and the ER sensors, the corrosion rate based on impedance sensor was integrated against time and converted into thickness loss, as shown in Fig. 9(a). It is seen that the calculated thickness loss curves by impedance sensors have similar trends during the wetting−drying cycling test, but there still exist big differences in corrosion thickness loss according to the above two methods. Table 2 summarizes the average corrosion rate of contaminated Cu by the impedance and ER sensors, and it is seen that with increasing drying time during each wetting−drying cycle, the average corrosion rate of Cu firstly increases and then decreases, among which the average corrosion rate reaches the highest value when the dry period increases to 10 h. The corrosion rate of Cu is significantly increased just in the drying period rather than wetting period, which is possibly attributed to the increasing oxygen diffusion rate and saline concentration with thinning TEL during the drying period. The moderately prolonged drying period may be beneficial to the thinning TEL and further the increasing corrosion rate of Cu. However, with further extension of drying period, the corrosion rate of Cu would be refrained due to the complete dehydration of corrosion sensors.

From Fig. 9(c), the corrosion rate obtained by ER sensor is 4−5 times higher than that by impedance sensor, mainly attributing to that the measured R_p at low frequency (0.01 Hz) in the dry period is much higher than the real R_p owing to lack

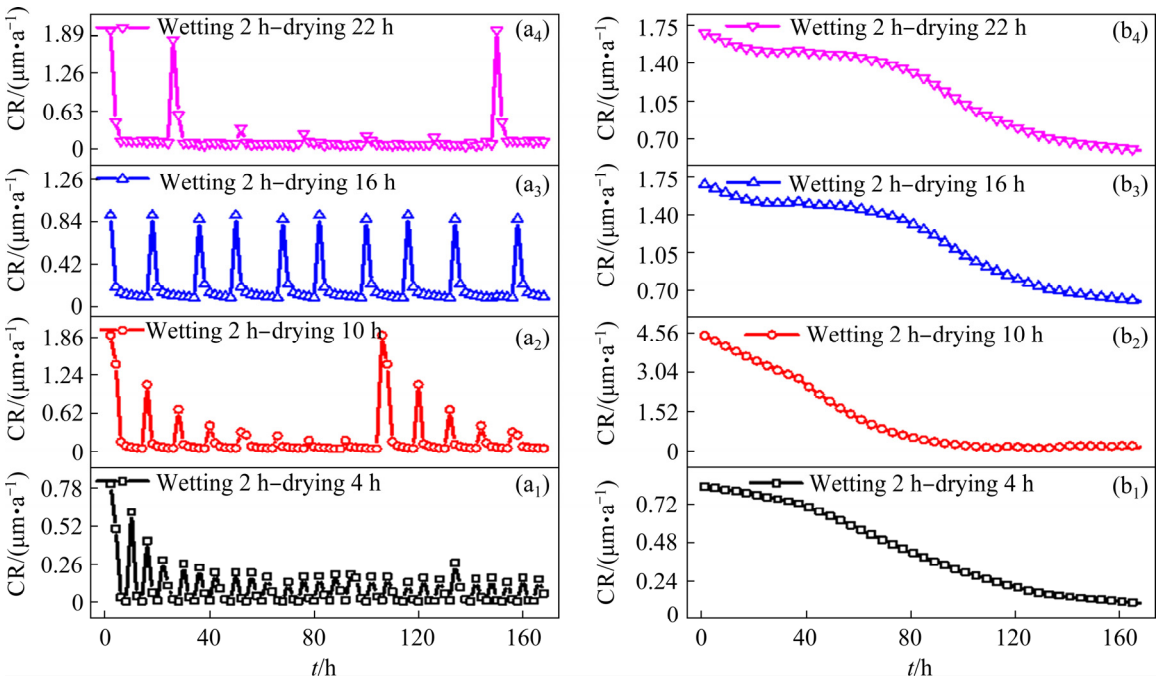

Fig. 8 Variations of instantaneous corrosion rate of NaCl-contaminated copper with time measured by impedance-based (a_1−a_4) and ER (b_1−b_4) sensors, firstly exposed in 90% RH and 35 °C air for 2 h, and then in 60% RH and 35 °C air for 4 h, 10 h, 16 h and 22 h, respectively (The wetting−drying cycle repeats until total time reaches 168 h)

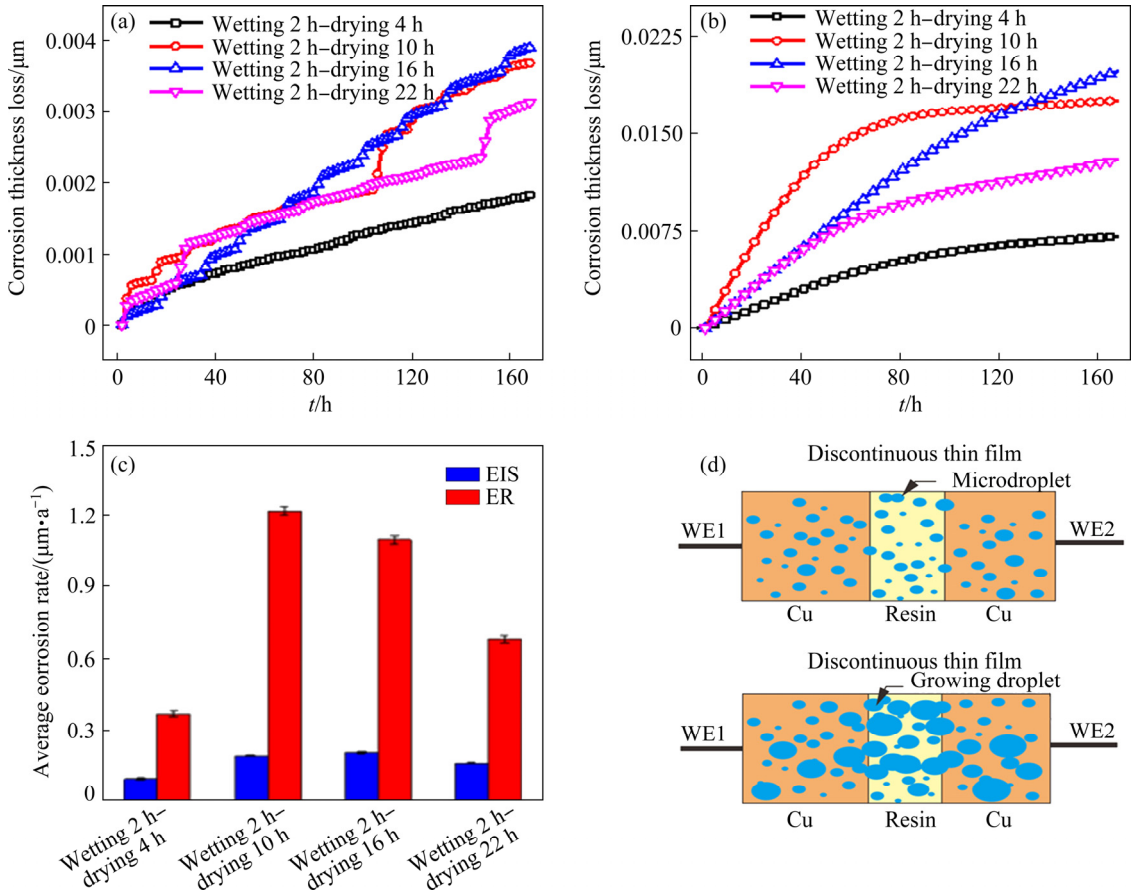

Fig. 9 Variations of thickness loss of NaCl-contaminated Cu with time measured by impedance (a) and ER sensors (b) under four wetting−drying cycling tests, and corresponding average corrosion rate (c) and schematic drying and wetting surface on impedance sensor

Table 2 Average corrosion rate obtained by impedance and ER sensors in wetting−drying cycle from Fig. 9

Monitoring technique	Average corrosion rate/(μm·a^{-1})			
	Wetting 2 h−drying 4 h	Wetting 2 h−drying 10 h	Wetting 2 h−drying 16 h	Wetting 2 h−drying 22 h
EIS	0.096±0.001	0.193±0.007	0.20±0.007	0.16±0.004
ER	0.43±0.008	1.24±0.01	1.15±0.009	0.77±0.009

of conductive bridge (continuous TEL) across the two comb-like Cu electrodes on the impedance sensor. According to Fig. 9(d), during the drying period, the TEL would become discontinuous, leading to the breakdown of conductive channel between the two working electrodes (WE1 and WE2). The impedance at 0.01 Hz only represents the impedance of disconnected TEL other than electrochemical reaction. Thus, the calculated corrosion rate based on the impedance sensor would be far lower than the real atmospheric corrosion rate of Cu owing to that most corrosion events occurring in a single Cu electrode fail to form a detectable current across the two WEs. Besides, the accurate value of B is exceedingly difficult to obtain, which may be another reason accounting for the different corrosion rates between impedance and ER sensors. Fortunately, for ER sensor, since it directly measures the thickness loss of Cu stripes according to the Ohmic law other than the electrochemical reaction, it is therefore unaffected by the discontinuous TEL during drying period.

The SEM images and XRD results of corrosion products formed on Cu specimens during the wetting−drying cycles are shown in Figs. 10 and 11, respectively. From Fig. 10(a), it is found that only a few of corrosion products appear on the Cu specimen surface, indicative of tiny corrosion of

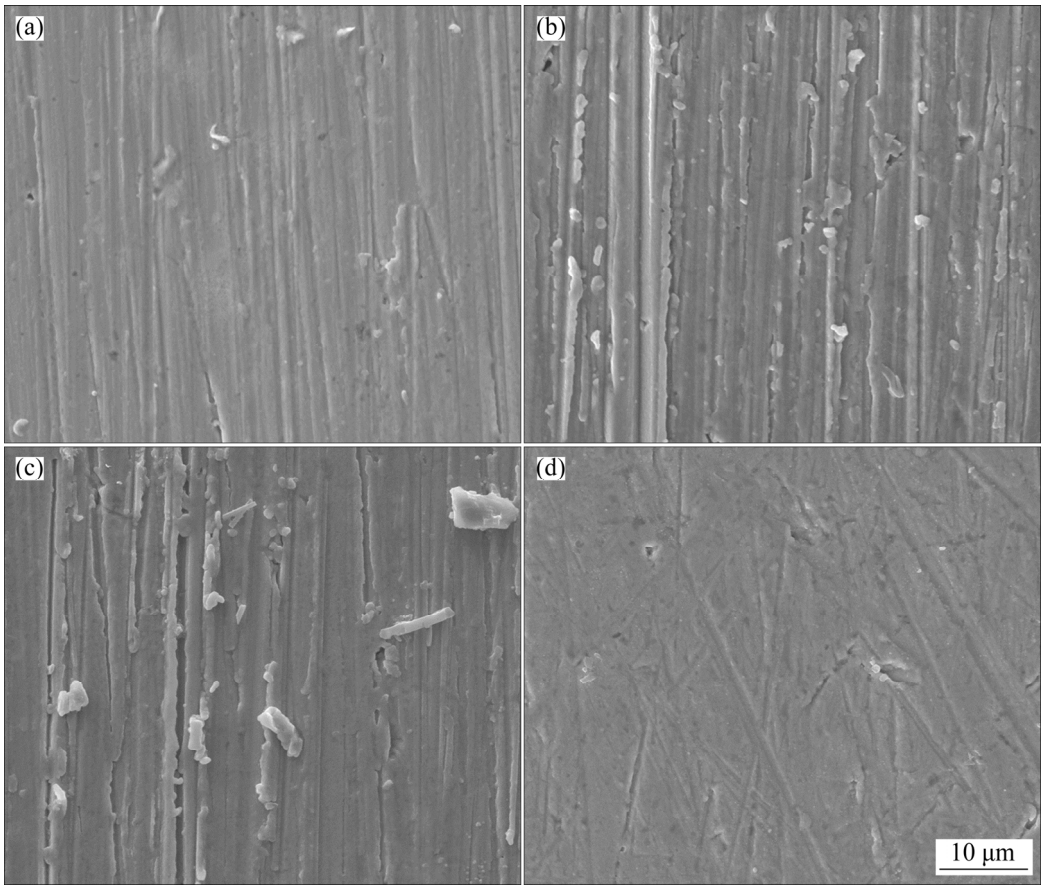

Fig. 10 Corrosion morphologies of contaminated copper after 168 h circulating exposure: firstly in 90% RH and 35 °C air for 2 h, and then in 60% RH and 35 °C air for 4 h (a), 10 h (b), 16 h (c) and 22 h (d)

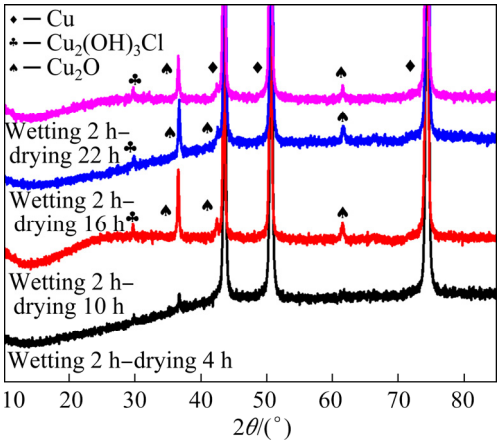

Fig. 11 XRD patterns of corrosion products for contaminated copper after 168 h circulating exposure: firstly in 90% RH and 35 °C air for 2 h, and then in 60% RH and 35 °C air for 4, 10, 16 and 22 h

Cu. With extended drying period, the accumulation amounts of corrosion products firstly increase and then decrease. When the drying period extends to 10 h in each wetting−drying cycle, the amount of corrosion products reaches their maximum, mainly scattering around the scratches on the Cu specimen. The SEM morphology of Cu corrosion products is in accordance with the corrosion rate by impedance and ER sensors. From Fig. 11, when the drying period is prolonged to 4 h, there are four peaks appearing on the Cu surface, among which the three typical peaks at 43.3°, 50.4° and 70.1° correspond to elemental Cu, while the weak peak at 36.5° is associated to Cu_2O, suggesting the occurrence of slight corrosion on Cu specimen. With prolonging drying period, new peaks appear at 29.6° and 61.4°, possibly ascribed to the formation of $Cu_2(OH)_3Cl$ and Cu_2O, respectively. It suggests that the corrosion process is accelerated with prolonged drying period. In addition, the peak intensity of Cu_2O reaches its maximum when the drying period is 10 h, suggesting that the cyclic pattern composed of 2 h wetting period plus 10 h drying period exhibits the most intensive corrosion acceleration ability. Nevertheless, the compositions of corrosion products almost keep unchanged with further extension of drying time after 10 h.

3.3 Corrosivity of high−low temperature cyclic atmosphere

Figure 12 shows the corrosion rates of NaCl-contaminated Cu with time measured by impedance (a_1−a_4) and ER (b_1−b_4) sensors, firstly exposed in 60% RH and 45 °C air for 2 h, and then in 60% RH and 25 °C air for 4, 10, 16 and 22 h. From the corrosion rate curves, it is found that the trends of corrosion rate against time are consistent based on the above two sensors, but the values of corrosion rate measured by EIS sensor are lower than those by ER sensor in the same atmosphere.

Similarly, the corrosion rate of Cu electrode was further converted into its thickness loss of Cu and shown in Fig. 13(a). Compared with the thickness loss by ER sensor in Fig. 13(b), the calculated thickness loss by impedance sensor has similar trend versus time to the ER sensor during high−low temperature cycling test. Table 3 lists the difference of corrosion rate for contaminated Cu based on the impedance and the ER sensors. It is seen that, with increasing low−temperature period during the high−low temperature cycling tests, the average corrosion rate of Cu firstly increases and then decreases, among which the corrosion rate reaches its maximum when the low-temperature

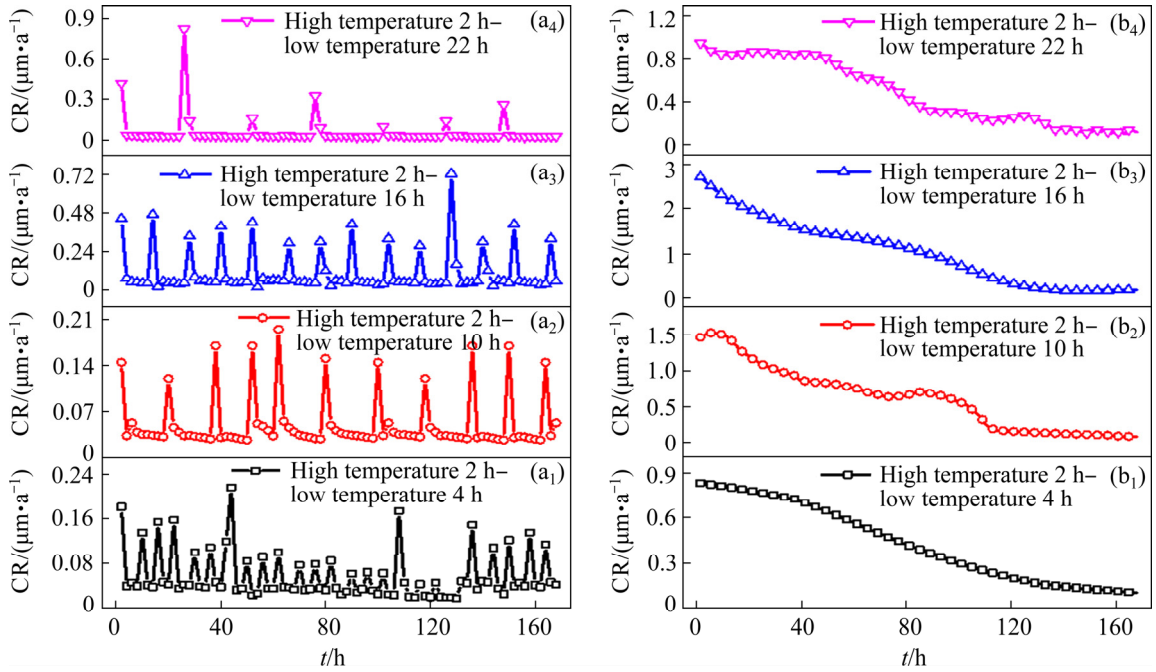

Fig. 12 Variations of instantaneous corrosion rate of NaCl-contaminated copper with time measured by impedance (a_1−a_4) and ER (b_1−b_4) sensors, firstly exposed in 60% RH and 45 °C air for 2 h, and then in 60% RH and 25 °C air for 4, 10, 16 and 22 h (The high−low temperature cycle repeats until total time reaches 168 h)

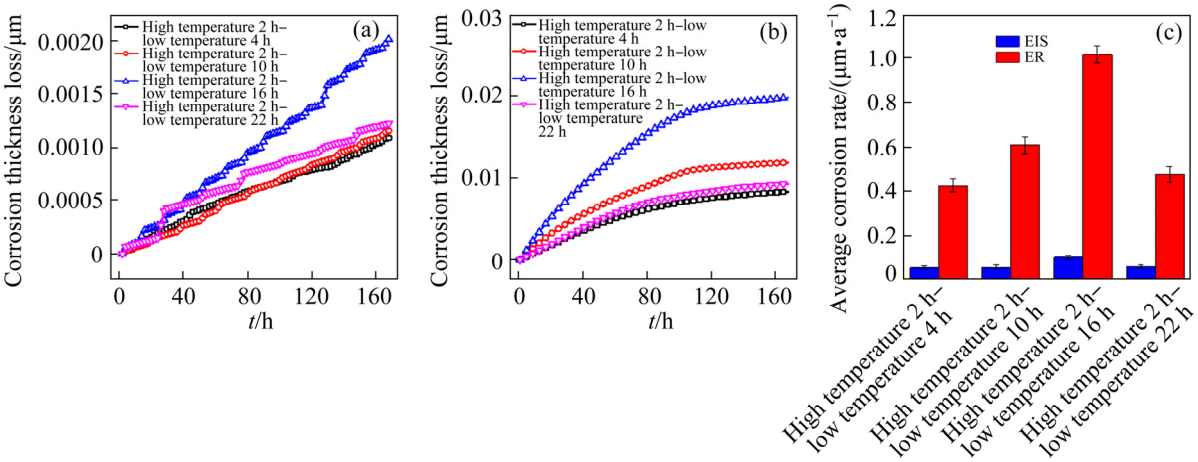

Fig. 13 Variations of corrosion thickness loss of NaCl-contaminated copper electrode with time measured by EIS (a) and ER (b) sensors under four high−low temperature cycling tests and their corresponding average corrosion rate (c)

period is 16 h during the high−low temperature cycle. The Cu corrosion rate is significantly increased during the cooling process due to that the water vapor condensation increases the thickness of TEL on Cu electrode. Moreover, moderately prolonging low-temperature period is beneficial to forming sufficient TEL, and thus accelerating the corrosion of Cu. However, with further extension of low-temperature period, the corrosion of Cu would be refrained owing to that electrochemical reaction is limited at low temperature.

From Fig. 13(c), the average corrosion rate obtained by ER sensor is 8−10 times higher than that by impedance sensor, mainly attributing to that the measured impedance at low frequency (0.01 Hz) during the drying period is higher than the real impedance because there is no conductive passage between two comb-like Cu electrodes on the impedance sensor in 60% RH air. When the impedance sensor becomes dry, the impedance at 0.01 Hz would become much higher. Thus, the values of corrosion rate from impedance sensor would be far lower than the real value. Besides, the selection of B value is another reason accounting for the different corrosion rates between impedance and ER sensors.

The SEM images and XRD results of corrosion products formed on Cu specimens during the high−low temperature cycles are shown in Figs. 14 and 15, respectively. From Fig. 14(a), it is

Table 3 Average corrosion rate obtained by impedance-based and ER sensors in high−low temperature cycling test from Fig. 13

Monitoring technique	Average corrosion rate/(μm·a^{-1})			
	High temperature 2 h−low temperature 4 h	High temperature 2 h−low temperature 10 h	High temperature 2 h−low temperature 16 h	High temperature 2 h−low temperature 22 h
EIS	0.056±0.001	0.059±0.002	0.10±0.003	0.063±0.002
ER	0.43±0.02	0.61±0.03	1.02±0.03	0.45±0.01

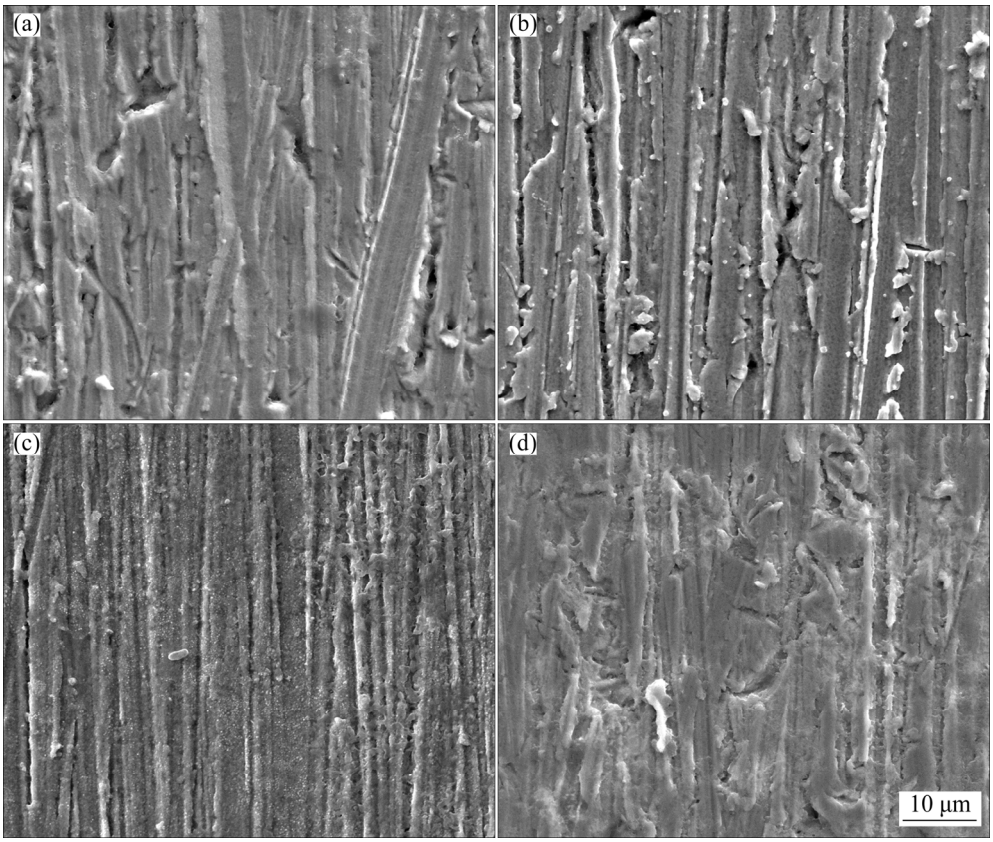

Fig. 14 Atmospheric corrosion morphologies of contaminated copper after 168 h cycling test: firstly in 60% RH and 45 °C air for 2 h, and then in 60% RH and 25 °C air for 4 h (a), 10 h (b), 16 h (c) and 22 h (d)

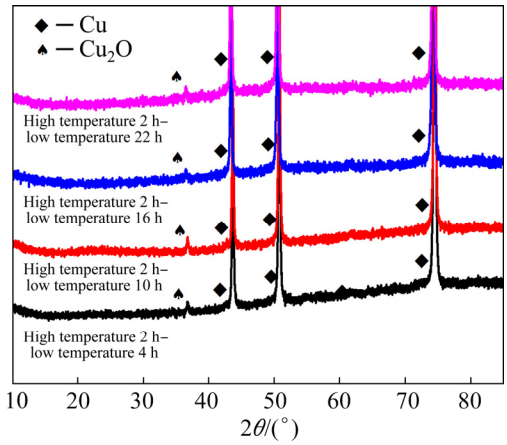

Fig. 15 XRD patterns of corrosion products of contaminated copper after 168 h cycling test: firstly in 60% RH and 45 °C air for 2 h, and then in 60% RH and 25 °C air for 4, 10, 16 and 22 h

found that only a few of corrosion products appear on the Cu specimen surface, and scratches could be obviously observed. With extended low temperature period during the high−low temperature cycling test, the accumulation amounts of corrosion products firstly increase and then decrease. When the low temperature period increases to 16 h, the amount of corrosion products reaches their maximum, which is in accordance with the corrosion rate results by impedance and ER sensors. Figure 15 shows the XRD patterns of corrosion products on NaCl-contaminated Cu surface after 168 h circling exposure: firstly in 60% RH and 45 °C air for 2 h, and then in 60% RH and 25 °C air for 4, 10, 16 and 22 h repeatedly. It could be seen that the composition of corrosion products almost keeps unchanged, only Cu_2O peak appearing at 36.5°.

4 Conclusions

(1) In the field station of atmospheric corrosion, corrosion rate measured by ER sensor is nearly consistent with that by weight loss method, which suggests that electrical resistance method could be used to effectively estimate the outdoor corrosion rate and corrosion thickness loss of Cu specimen.

(2) In the indoor wetting−drying/high−low temperature cycling tests, corrosion rate and thickness loss of Cu electrode measured by impedance sensor have similar trend with those obtained by ER sensor, but the latter is much higher than the former. It is mainly attributed to that electrochemical impedance method fails to indicate the real polarization resistance of Cu under discontinuous TEL owing to lack of conductive passage between two interlaced electrodes.

(3) ER method is more suitable for atmospheric corrosion monitoring than electrochemical impedance method. Compared with ER technique, the electrochemical impedance technique could sensitively reflect the time of wetting on Cu specimen surface.

Acknowledgments

The authors want to thank the financial supports from the National Natural Science Foundation of China (No. 51771079), and the China Postdoctoral Science Foundation (No. 2020M682650).

References

[1] HUANG Hua-liang, DONG Ze-hua, CHEN Zhen-yu, GUO Xing-peng. The effects of Cl^- ion concentration and relative humidity on atmospheric corrosion behaviour of PCB-Cu under adsorbed thin electrolyte layer [J]. Corrosion Science, 2011, 53(4): 1230−1236.

[2] KRAEMER F, ROELLIG M, METASCH R, AHMAR J, MEIER K, WIESE S. Experimental determination of the Young's modulus of copper and solder materials for electronic packaging [J]. Microelectronics Reliability, 2018, 91: 251−256.

[3] PAN M Y, GUPTA M, TAY A A O, VAIDYANATHAN K. Development of bulk nanostructured copper with superior hardness for use as an interconnect material in electronic packaging [J]. Microelectronics Reliability, 2006, 46(5): 763−767.

[4] MOKHLIS H, DAOUDI R, AZZI M. Study of the electrochemical behavior of printed circuit boards (PCBs) leaching solutions using glycine and copper recovery by electrodeposition from leachate solutions [J]. Materials Today: Proceedings, 2021, 37(3): 3973−3979.

[5] ZHI Yuan-jie, JIN Zhi-hui, LU Lin, YANG Tao, ZHOU De-yun, PEI Zi-bo, WU De-quan, FU Dong-mei, ZHANG Da-wei, LI Xiao-gang. Improving atmospheric corrosion prediction through key environmental factor identification by random forest-based model [J]. Corrosion Science, 2021, 178: 109084.

[6] KATONA R, KELLY R, BRYAN C, SCHALLER R, KNIGHT A. Use of in situ Raman spectroelectrochemical technique to explore atmospheric corrosion in marine-relevant environments [J]. Electrochemistry Communications, 2020, 118: 106768.

[7] EMETERE M, OKORO E, AKINLABI E, SANNI S. Effect of atmospheric aerosol on corrosion of metallic surfaces [J].

Procedia Manufacturing, 2019, 35: 666−673.

[8] CAI Yi-kun, ZHAO Yu, MA Xiao-bing, ZHOU Kun, CHEN Yuan. Influence of environmental factors on atmospheric corrosion in dynamic environment [J]. Corrosion Science, 2018, 137: 163−175.

[9] HUANG Hua-liang, GUO Xing-peng, ZHANG Guo-an, DONG Ze-hua. Effect of direct current electric field on atmospheric corrosion behavior of copper under thin electrolyte layer [J]. Corrosion Science, 2011, 53(10): 3446−3449.

[10] HUANG Hua-liang, GUO Xing-peng, BU Fu-rong, HUANG Gang-liang. Corrosion behavior of immersion silver printed circuit board copper under a thin electrolyte layer [J]. Engineering Failure Analysis, 2020, 117: 104807.

[11] SALAHINEJAD E, ESLAMI-FARSANI R, TAYEBI L. Corrosion failure analysis of printed circuit boards exposed to H_2S-containing humid environments [J]. Engineering Failure Analysis, 2017, 79: 538−546.

[12] QIAO Chuang, WANG Ming-na, HAO Long, LIU Xia-he, JIANG Xiao-lin, AN Xi-zhong, LI Duan-yang. Temperature and NaCl deposition dependent corrosion of SAC305 solder alloy in simulated marine atmosphere [J]. Journal of Materials Science & Technology, 2021, 75: 252−264.

[13] HUANG Hua-liang, GUO Xing-peng, ZHANG Guo-an, DONG Ze-hua. The effects of temperature and electric field on atmospheric corrosion behaviour of PCB-Cu under absorbed thin electrolyte layer [J]. Corrosion Science, 2011, 53(5): 1700−1707.

[14] VOGEL G. Creeping corrosion of copper on printed circuit board assemblies [J]. Microelectronics Reliability, 2016, 64: 650−655.

[15] ZOU Shi-wen, LI Xiao-gang, DONG Chao-fang, DING Kang-kang, XIAO Kui. Electrochemical migration, whisker formation, and corrosion behavior of printed circuit board under wet H_2S environment [J]. Electrochimica Acta, 2013, 114: 363−371.

[16] CHEN Z, PERSSON D, LEYGRAF C. Initial NaCl-particle induced atmospheric corrosion of zinc—Effect of CO_2 and SO_2 [J]. Corrosion Science, 2008, 50(1): 111−123.

[17] KOUSHIK B, STEEN N, MAMME M, INGELGEM Y, TERRYN H. Review on modelling of corrosion under droplet electrolyte for predicting atmospheric corrosion rate [J]. Journal of Materials Science & Technology, 2021, 62: 254−267.

[18] THEE C, HAO Long, DONG Jun-hua, MU Xin, WEI Xin, LI Xiao-fang, KE Wei. Atmospheric corrosion monitoring of a weathering steel under an electrolyte film in cyclic wet–dry condition [J]. Corrosion Science, 2014, 78: 130−137.

[19] YADAV A P, NISHIKATA A, TSURU T. Electrochemical impedance study on galvanized steel corrosion under cyclic wet–dry conditions—Influence of time of wetness [J]. Corrosion Science, 2004, 46(1): 169−181.

[20] LIAO Bo-kai, WANG Hong, XIAO Wei-ping, YU Cai, GUO Xing-peng. Recent advances in method of suppressing dendrite formation of tin-based solder alloys [J]. Journal of Materials Science: Materials in Electronics, 2020, 31(16): 13001−13010.

[21] PEI Zi-bo, CHENG Xue-qun, YANG Xiao-jia, LI Qing, XIA Chen-han, ZHANG Da-wei, LI Xiao-gang. Understanding environmental impacts on initial atmospheric corrosion based on corrosion monitoring sensors [J]. Journal of Materials Science & Technology, 2021, 64: 214−221.

[22] JIN Yong-hee, HA Min-gyun, JEON Seok-hyeon, JEONG Young-soo, AHN Jin-hee. Evaluation of corrosion conditions for the steel box members by corrosion monitoring exposure test [J]. Construction and Building Materials, 2020, 258: 120195.

[23] MANSFELD F, KENKEL J. Electrochemical monitoring of atmospheric corrosion phenomena [J]. Corrosion Science, 1976, 16(3): 111−122.

[24] MANSFELD F, TSAI S. Laboratory studies of atmospheric corrosion—I. Weight loss and electrochemical measurements [J]. Corrosion Science, 1980, 20(7): 853−872.

[25] MANSFELD F, VIJAYAKUMAR R. Atmospheric corrosion behavior in Southern California [J]. Corrosion Science, 1988, 28(9): 939−946.

[26] MIZUNO D, SUZUKI S, FUJITA S, HARA N. Corrosion monitoring and materials selection for automotive environments by using Atmospheric Corrosion Monitor (ACM) sensor [J]. Corrosion Science, 2014, 83: 217−225.

[27] HUTTUNEN-SAARIVIRTA E, RAJALA P, BOMBERG M, CARPÉN L. EIS study on aerobic corrosion of copper in ground water: Influence of micro-organisms [J]. Electrochimica Acta, 2017, 240: 163−174.

[28] PAN Chen, LV Wang-yan, WANG Zhen-yao, SU Wei, WANG Chuan, LIU Shi-nian. Atmospheric corrosion of copper exposed in a simulated coastal-industrial atmosphere [J]. Journal of Materials Science & Technology, 2017, 33(6): 587−595.

[29] GANBORENA L, VEGA J M, ÖZKAYA B, GRANDE H, GARCÍA-LECINA E. An SKP and EIS study of microporous nickel-chromium coatings in copper containing electrolytes [J]. Electrochimica Acta, 2019, 318: 683−694.

[30] NISHIKATA A, SUZUKI F, TSURU T. Corrosion monitoring of nickel-containing steels in marine atmospheric environment [J]. Corrosion Science, 2005, 47(10): 2578−2588.

[31] LI Chun-ling, MA Yuan-tai, LI Ying, WANG Fu-hui. EIS monitoring study of atmospheric corrosion under variable relative humidity [J]. Corrosion Science, 2010, 52(11): 3677−3686.

[32] WAN Shan, HOU Jian, ZHANG Ze-fan, ZHANG Xin-xin, DONG Ze-hua. Monitoring of atmospheric corrosion and dewing process by interlacing copper electrode sensor [J]. Corrosion Science, 2019, 150: 246−257.

[33] KOURIL M, PROSEK T, SCHEFFEL B, DEGRES Y. Corrosion monitoring in archives by the electrical resistance technique [J]. Journal of Cultural Heritage, 2014, 15(2): 99−103.

[34] LI S Y, KIM Y G, JUNG S S, SONG H S, LEE S M. Application of steel thin film electrical resistance sensor for in situ corrosion monitoring [J]. Sensors and Actuators B: Chemical, 2007, 120(2): 368−377.

[35] RODRIGUES R, GABOREAU S, GANCE J, IGNATIADIS I, BETELU S. Reinforced concrete structures: A review of corrosion mechanisms and advances in electrical methods for

corrosion monitoring [J]. Construction and Building Materials, 2021, 269: 121240.
[36] CAI J, LYON S. A mechanistic study of initial atmospheric corrosion kinetics using electrical resistance sensors [J]. Corrosion Science, 2005, 47(12): 2956−2973.
[37] PROSEK T, TAUBE M, DUBOIS F, THIERRY D. Application of automated electrical resistance sensors for measurement of corrosion rate of copper, bronze and iron in model indoor atmospheres containing short-chain volatile carboxylic acids [J]. Corrosion Science, 2014, 87: 376−382.
[38] SCHINDELHOLZ E, KELLY R, COLE I, GANTHER W, MUSTER T. Comparability and accuracy of time of wetness sensing methods relevant for atmospheric corrosion [J]. Corrosion Science, 2013, 67: 233−241.

基于电化学阻抗和电阻传感器对比研究铜的大气腐蚀

万 闪[1]，廖伯凯[1]，董泽华[2]，郭兴蓬[1,2]

1. 广州大学 化学化工学院，广州 510006；
2. 华中科技大学 化学与化工学院 湖北省材料化学与服役失效重点实验室，武汉 430074

摘 要：开发电化学阻抗和薄膜电阻传感器，用于干湿/高低温循环加速试验和现场暴露试验中铜的大气腐蚀测量。三个月的场外暴露试验结果表明，电阻传感器测量的铜平均腐蚀速率与失重法得到的腐蚀速率基本一致。在干湿循环试验中，电化学阻抗传感器可灵敏地反映传感器表面的潮湿/干燥时间。尽管电化学阻抗传感器测得的平均腐蚀速率与电阻传感器测得的腐蚀速率具有相似的趋势，但前者测量结果对环境湿度的依赖性较后者大。当相对湿度低于 60%时，通过电化学阻抗法得到的平均腐蚀速率远低于失重法的，这主要归因于低湿度条件下梳齿铜电极之间无法形成连续导电的薄液膜通道，导致电化学阻抗传感器无法检测到电流信号。与电化学方法相比，电阻法更适合大气腐蚀监测，因为无论电阻传感器表面潮湿或者干燥，它都能根据欧姆定律灵敏地监测铜箔的厚度损失。

关键词：大气腐蚀；铜；电阻探针；电化学阻抗；原位腐蚀监测

(Edited by Xiang-qun LI)